*Laser Physics, Vol. 13, No. 12, 2003, pp. 1467–1477.*




# Magnetic Field-Induced Mixing of Hyperfine States of the Cs $6_2P_{3/2}$ Level Observed with a Submicron Vapor Cell

**A. V. Papoyan[1], D. H. Sarkisyan[1], K. Blush[2], M. Auzinsh[2], D. Bloch[3], and M. Ducloy[3]**

[1] *Institute for Physical Research, Armenian National Academy of Sciences, Ashtarak-2, 378410 Armenia*
[2] *Department of Physics, University of Latvia, 19 Rainis blvd., Riga, LV-1586, Latvia*
[3] *Labaratoire de Physique des Lasers, UMR 7538 du CNRS, Institut Galilee, Université Paris-Nord, 93430 Villetaneuse, France*

e-mail: papoyan@ipr.sci.am

Received February 5, 2003

**Abstract**—The fluorescence spectra of a submicron atomic cesium vapor layer observable under resonant excitation on the D2 line are studied in the presence of an external magnetic field. Substantial changes in the amplitudes and frequency positions of individual hyperfine transitions (resolved using a 300-nm-long vapor cell) were recorded in moderate magnetic fields (up to ~50 Gauss). These features are caused by mixing of the hyperfine states of the upper level resulting from comparable values of the hyperfine splitting of the $6^2P_{3/2}$ manifold and Larmor frequencies of the magnetic sublevels. The results of simulation show good agreement with the experimental spectra. Possible application of the results for high spatial resolution magnetometry is discussed.

## 1. INTRODUCTION

It is well known that the application of an external magnetic field modifies the absorptive and dispersive properties of an atomic system. As the magnetic field strength starts to increase from the zero value, the degeneracy of atomic states lifts and magnetic sublevels diverge. A linear shift of these sublevels takes place until the $B$ field reaches values for which the Zeeman splitting becomes comparable to the hyperfine splitting of atomic levels. In this regime, the wavefunctions of the hyperfine manifold begin to mix with each other. This mixing results in dual consequences. First, the shift of the magnetic sublevels is no longer linear on the $B$ field (and of different behavior for different individual sublevels). Second, the probabilities of the optical transitions between the magnetic sublevels of the lower and upper atomic states differ from unperturbed values [1]. For the first excited levels of Rb and Cs, atoms of particular interest in spectroscopic studies, the linear Zeeman regime ends at $B < 100$ Gauss. Thus, the crossing of magnetic sublevels for the $5^2P_{3/2}$ manifold of $^{85}$Rb occurs at $B \approx 4$ Gauss [2]. Since magnetic splitting in these conditions is incomparably smaller than Doppler broadening, direct observation of hyperfine sublevels mixing effects in absorption and fluorescence spectra for vapor media becomes rather complicated. This is why studies have been carried out either for higher magnetic fields [1] or at lower magnetic fields by nondirect methods, such as selective reflection spectroscopy [3, 4] and magnetooptical rotation near the resonance line (see [5] and references therein). Also, the alignment to orientation conversion can be used as a very sensitive tool to study level mixing due to different perturbations (see [6, 7] and references therein), including atoms with hyperfine structure in a magnetic field [2].

The development of extremely thin vapor cells (ETC) of submicron thickness [8] has opened new possibilities for high resolution spectroscopy of vapor (gaseous) media, allowing one to directly record sub-Doppler lines in the fluorescence and transmission spectra. In particular, as is shown in [8], all six hyperfine transitions of the Cs atomic D2 line are completely resolved in the fluorescence spectrum (Fig. 1 shows hyperfine levels and transitions relevant for this line). Moreover, it should be noted that the amplitude ratios for the individual hyperfine transitions are practically independent of the intensity of exciting radiation. The latter indicates that the depopulation by optical pump-

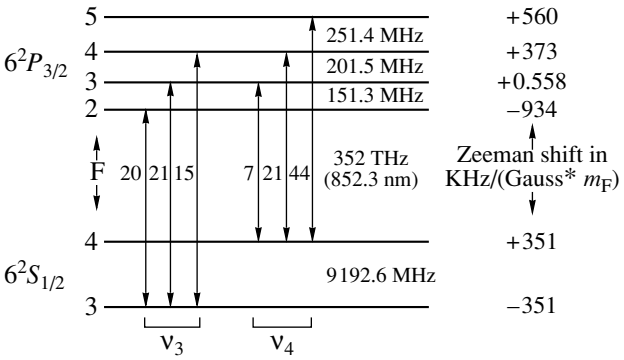


**Fig. 1.** Relevant energy levels for the D2 line of Cs including hyperfine structure and relative transition probability.

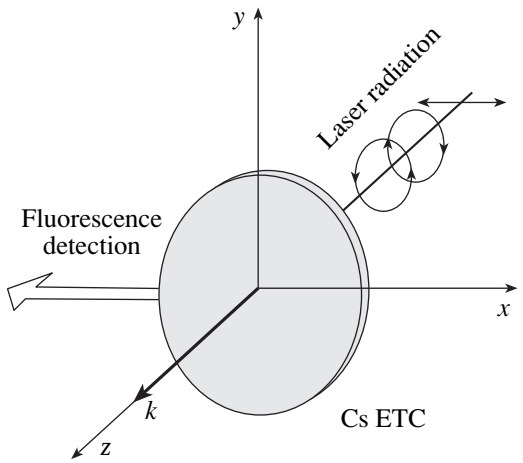


**Fig. 2.** Geometrical configuration of the experiment. Laser radiation propagation **k** along the *z* axis; arrows show various polarization cases (linear, circular left- and right-handed). Magnetic field applied along the *x*, *y*, or *z* axis. Cs ETC: extremely thin (submicron) cell containing Cs vapor.

ing on the noncycling transitions $F_g = 3, 4 \longrightarrow F_e = 3, 4$ is not established even at laser intensities of $I_L \sim 50$ mW/cm$^2$ for the submicron vapor column length. This property is of importance for quantitative spectroscopic and magnetooptical measurements.

Absorption and emission processes in the submicron-thick dilute vapor layer are strongly affected by an anisotropic geometrical factor. For the atoms moving at a mean thermal velocity normal to the window surface (that is, in the Doppler-sensitive direction), the wall-to-wall flight tune is only ~1 ns, i.e., much less than the inverse natural width of the optical transition. Fast atoms simply do not have time to absorb and, especially, to emit radiation before getting de-excited on the dielectric surface. As a result, the contribution of slow longitudinal velocity atoms in the spectra becomes predominant, giving rise to Dicke-type sub-Doppler features [9]. Moreover, since the use of the ETC allows one to substantially diminish the Doppler broadening of spectral lines, the influence of the magnetic field on individual hyperfine components can be revealed at weaker magnetic fields as compared with well-known experiments on upper-state level mixing and crossing in Doppler-broadened gases. Hence, the gradual **I**–**J** decoupling as a magnetic field is increased can be studied in detail.

Up to now, magnetic field–induced effects in thin cells of radiation-wavelength-scale thickness have been studied only theoretically [10]. In this study, peculiarities of Faraday rotation and magnetic circular dichroism have been considered.

In the present work, we have studied the influence of a magnetic field on the fluorescence spectra of a submicron Cs vapor layer. The choice of fluorescence rather than absorption studies was justified by the better spectral resolution of individual hyperfine lines [8].

## 2. EXPERIMENTAL

A schematic drawing of the measurement configuration is shown in Fig. 2. The radiation beam ($\varnothing$ = 3 mm) of a single-frequency cw laser diode with $\lambda$ = 852 nm and a linewidth of 20 MHz was directed at normal incidence onto ETCs ~300 nm in thickness with the side arm containing cesium. The cell was placed inside three pairs of mutually perpendicular Helmholtz coils, which made it possible to cancel the earth magnetic field and to apply a homogeneous magnetic field in an arbitrary direction. The laser frequency was linearly scanned in the region of $\nu_3$ or $\nu_4$ transitions of a Cs atom (Fig. 1). A Glan–Thomson prism was used to purify the original (linear) radiation polarization of the laser diode; to produce a circular polarization, a $\lambda/4$ plate was utilized. A photodiode followed by an operation amplifier was placed at 90° to the direction of laser propagation to detect the fluorescence signal emerging through one of two side openings of the cell oven. The photodiode collected fluorescence emission within ~0.1 sr solid angle.

The intensity of the fluorescence emission in the direction of the *x* axis [see Fig. 2] (with no spectral or polarization analysis) from the vapor layer excited by linearly (along the *x* axis) or circularly polarized radiation was recorded versus the laser radiation frequency for various directions and magnitudes of the external magnetic field. For the case of a longitudinal magnetic field (**B**//**k**), right- and left-handed circular (elementary) polarizations are denoted as $\sigma^+$ and $\sigma^-$, respectively. As one could expect, switching from $\sigma^+(\sigma^-)$ to $\sigma^-(\sigma^+)$ by adjusting the $\lambda/4$ plate keeping the direction of the magnetic field $+B$ invariable in this case was completely identical to switching the magnetic field from $+B$ to $-B$ keeping the polarization helicity $\sigma^+(\sigma^-)$ invariable. Indeed, the recorded signals in these two cases were the same and, for technical convenience, the second option has been exploited for the regular measurements. Over 80 experimental spectra have been recorded with the *B* field strength ranging from 0 to 55 Gauss (the maximum field produced by the set of Helmholtz coils we used) with the step of 11 Gauss. In fact, some influence from the magnetic field is clearly observable already at $B \sim 10$ Gauss, but to avoid cumbersome graphical presentation we will restrict ourselves by the limiting cases of $B = 0$ and $B = 55$ Gauss (in the latter case, the effect of the *B* field is the most visible).

Scatter circles in Figs. 3–5 show examples of the recorded fluorescence spectra. The orientations of the *B* field are $B = B_z$ (Fig. 3), $B = B_x$ (Fig. 4), and $B = B_y$ (Fig. 5). Figures 3a, 4a, and 5a represent the results for $\nu_4$ transitions ($F_g = 4 \longrightarrow F_e = 3, 4, 5$), and Figs. 3b, 4b, and 5b show the results for $\nu_3$ transitions ($F_g = 3 \longrightarrow$

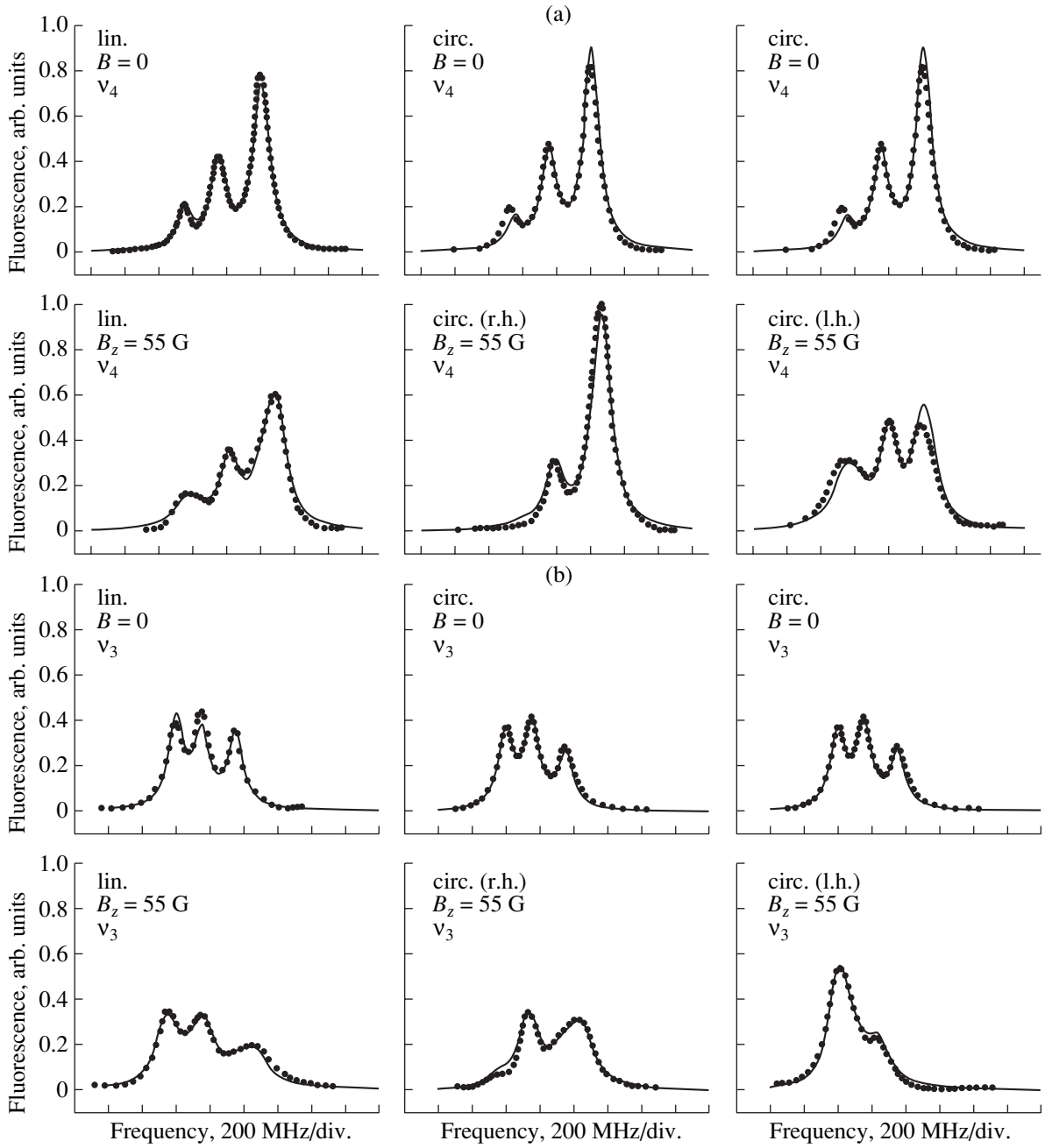


**Fig. 3.** Experimental (scatter circles) and theoretical (lines) fluorescence spectra of (a) $\nu_4$: $F_g = 4 \longrightarrow F_e = (2), 3, 4, 5$ and (b) $\nu_3$: $F_g = 3 \longrightarrow F_e = 2, 3, 4, (5)$ transitions without a magnetic field (upper row) and with a magnetic field of $B_z = 55$ Gauss (lower row). Incident radiation polarization: linear (left column), circular right-handed (middle column), and left-handed (right column). The frequency increases rightwards; the arbitrary units of the vertical (intensity) axis are the same for all graphs.

$F_e = 2, 3, 4$).[1] In all the figures, the upper rows in the graphs are $B = 0$ spectra and the lower row graphs are $B = 55$ Gauss spectra. Notations for every column indicate the applied laser radiation polarization and $B$-field orientation. In fact, for the given laser radiation intensity and observation direction, the fluorescence spectrum at $B = 0$ depends only on the polarization of laser radiation and only two (different from each other) spectra are presented in the upper rows of all the graphs in Figs. 3–5, i.e., for linear and circular polarization. They

[1] These notations are valid for $B = 0$. As **I**–**J** decoupling starts to develop in the $B$ field, the levels that initially are not accessible due to dipole transition selection rules start to contribute to optical transitions. Hence, it would be more correct to write $F_g = 3 \longrightarrow F_e = 2, 3, 4, (5)$ for $\nu_3$ and $F_g = 4 \longrightarrow F_e = (2), 3, 4, 5$ for $\nu_4$.

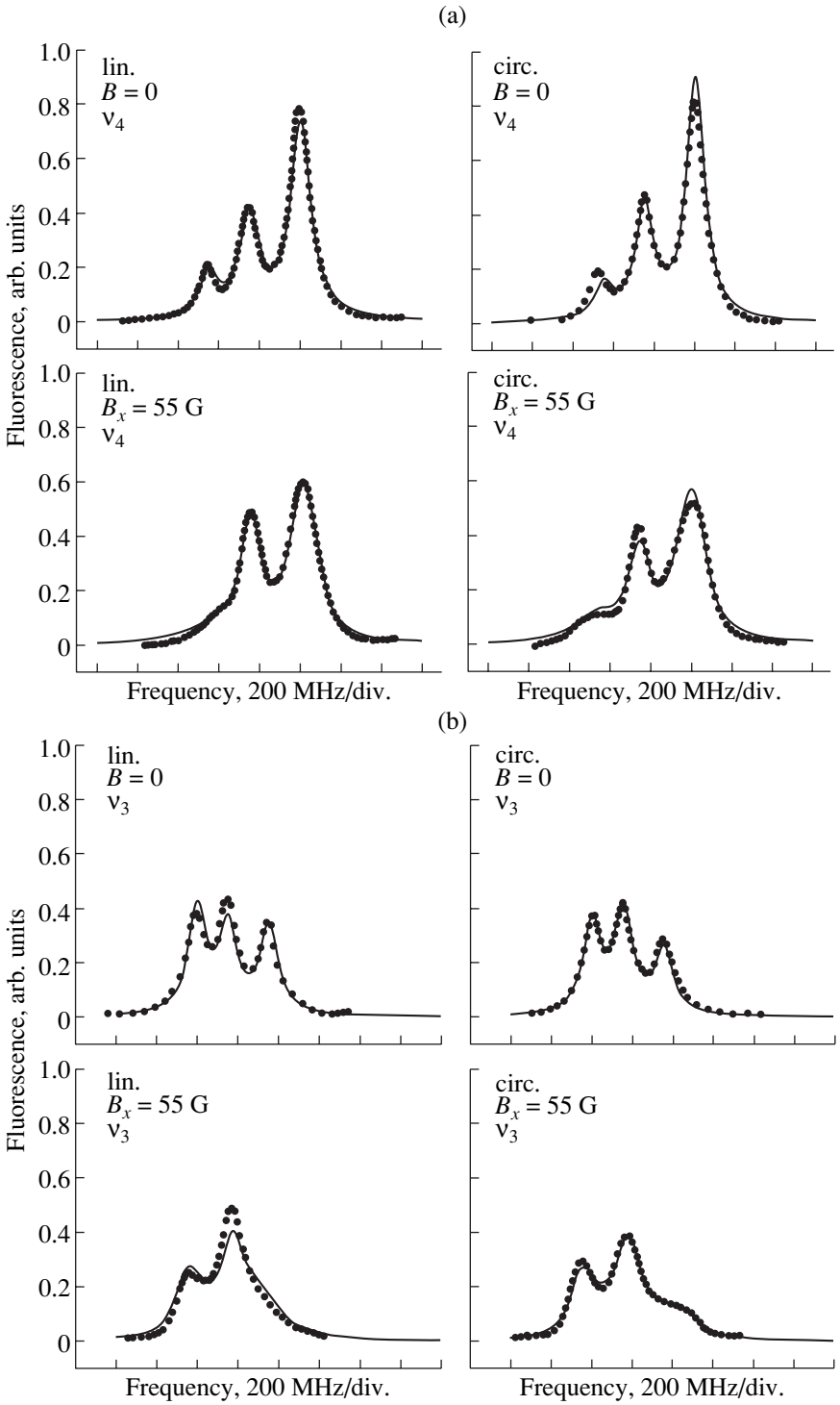


**Fig. 4.** Experimental (scatter circles) and theoretical (lines) fluorescence spectra of (a) $\nu_4$: $F_g = 4 \longrightarrow F_e = (2), 3, 4, 5$ and (b) $\nu_3$: $F_g = 3 \longrightarrow F_e = 2, 3, 4, (5)$ transitions without a magnetic field (upper row) and with a magnetic field of $B_x = 55$ Gauss (lower row). Incident radiation polarization: linear (left column) and circular (right column). The frequency increases rightwards; the arbitrary units of the vertical (intensity) axis are the same for all graphs.

are repeated simply to stress the modifications induced by a magnetic field in each particular case (for visual comparison). The vertical (intensity) scale is the same for all the graphs. The horizontal (frequency) scale is 200 MHz/div.; the frequency rises rightwards. The saturated absorption signal from a 1.5-cm-long auxiliary

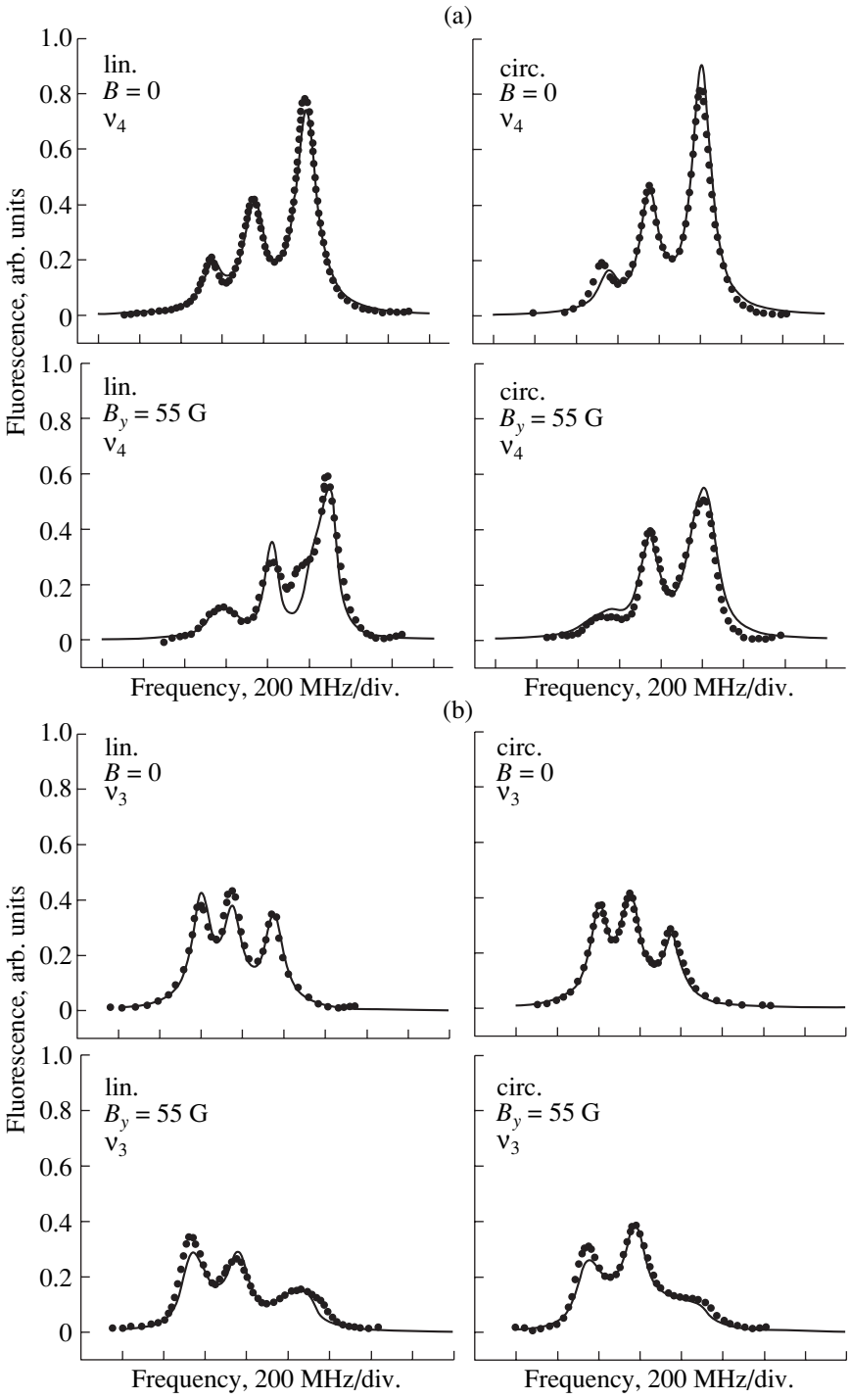


**Fig. 5.** Experimental (scatter circles) and theoretical (lines) fluorescence spectra of (a) $\nu_4$: $F_g = 4 \longrightarrow F_e = (2), 3, 4, 5$ and (b) $\nu_3$: $F_g = 3 \longrightarrow F_e = 2, 3, 4, (5)$ transitions without a magnetic field (upper row) and with a magnetic field of $B_y = 55$ Gauss (lower row). Incident radiation polarization: linear (left column) and circular (right column). The frequency increases rightwards; the arbitrary units of the vertical (intensity) axis are the same for all graphs.

Cs cell was used as a frequency marker (reference). The temperature of the side arm reservoir of the cell (the latter defined the saturated vapor pressure) was kept at $T_r = 105°C$ throughout the measurements. The corresponding number density of Cs atoms is $N_{Cs} = 2 \times 10^{13}$ cm$^{-3}$, and the width of collisional (homogeneous)

broadening of the spectral lines is ≈1.8 MHz, i.e., nearly three times smaller than for the natural linewidth. The Doppler (inhomogeneous) linewidth in this temperature regime is ≈440 MHz.

In agreement with the nearly linear intensity dependence of fluorescence reported in [8], the shape of the fluorescence spectrum does not noticeably depend on the intensity of laser radiation, at least, not in the range of $I_L$ = 1–50 mW/cm$^2$. All the spectra presented in the graphs were recorded with $I_L$ = 40 mW/cm$^2$. For $I_L$ < 1 mW/cm$^2$, the fluorescence signal is too weak to be recorded. On the other hand, focusing of the laser beam is required to get higher laser intensities $I_L$ > 50 mW/cm$^2$, but in this case the interaction time (time of flight) changes simultaneously; focusing also decreases the number of atoms contributing to the fluorescence signal. The spectra remain invariable under reversal of the direction of laser frequency scanning. A substantial difference in spectra for right-handed ($\sigma^+$) and left-handed ($\sigma^-$) circular polarizations of the laser radiation is observed only for longitudinal direction of the $B$ field ($B = B_z$, Fig. 3). For the case of a transverse magnetic field (Figs. 4, 5), the helicity of light is of no relevance and the corresponding spectra are identical. Moreover, the spectra with circularly polarized excitation for $B = B_x$ (Fig. 4) and $B = B_y$ (Fig. 5) are practically identical. These observations are easily understandable reasoning from the symmetry.

As we can see from Figs. 3–5, the individual magnetic subtransitions $m_{Fg} \longrightarrow m_{Fe}$ of the same hyperfine transition $F_g \longrightarrow F_e$ are not resolved in the conditions of the present experiment. Indeed, in the case of complete resolution, one could expect to see 18 magnetic transitions for the $\nu_3$ line and 24 magnetic transitions for the $\nu_4$ line for each elementary polarization: $\pi$ (linear, **B**//**E**), $\sigma^+$ and $\sigma^-$ (circular, **B**//**k**), and up to 88 magnetic transitions for more complex $B$-field orientation cases. The results of the experiment can be interpreted rather as a $B$-field orientation- and magnitude-dependent frequency shift and variation in amplitude of the $F_g \longrightarrow F_e$ hyperfine transitions.

We would like to draw special attention to the results depicted in Fig. 3, with dramatic difference between the fluorescence spectra for the $\sigma^+$ and $\sigma^-$ polarizations. This nonintuitive behavior reflects the magnetic circular dichroism of Cs atoms (i.e., different absorption coefficients for $\sigma^+$ and $\sigma^-$ light in the magnetic field). The most surprising result is that the $F_g = 4 \longrightarrow F_e = 3$ (Fig. 3a, $\sigma^+$ (right-handed) polarization) and $F_g = 3 \longrightarrow F_e = 4$ (Fig. 3b, $\sigma^-$ (left-handed) polarization) are found to be completely suppressed at rather low magnetic fields.

## 3. MODEL

We will use the following model to simulate the spectra of the Cs atomic film without a magnetic field and with a magnetic field. First, we will assume that the absorption rate $\Gamma_p$ is small in comparison with the relaxation rates in the ground and excited states, denoted by $\gamma$ and $\Gamma$, respectively: $\Gamma_p < \gamma, \Gamma$. This assumption is well justified by the observation of the fluorescence spectrum being independent of laser intensity. Second, in so far as the laser linewidth is rather broad ($\Delta\nu_L \approx 20$ MHz), the spectral radiation that excites atoms is broader than the homogeneous width of the atomic transition: the radiation width of the transition is $\Gamma_{rad} = 1/(2\pi\tau) \approx 5.2$ MHz, where $\tau \approx 30.5$ ns is the lifetime of Cs in the $6^2P_{3/2}$ state [11]. These conditions correspond to the broad line approximation, for which the correlation time of the optical dipole, imposed by the inverse laser linewidth, is short with respect to the excited state decay time [12].

As we will see further, the conditions for laser excitation of atoms differ substantially when the magnetic field is switched off and when it is applied. Let us start with the analysis of the excitation of atoms in a zero magnetic field.

### *3.1. Zero Magnetic Field Signal*

A convenient way to describe excited state–atom optical excitation in the broad line approximation is by means of a quantum density matrix $f_{mm'}$ [12, 13]. We will consider an atom that absorbs laser light polarized in a direction characterized by the light electric field vector $\mathbf{E}_{exc}$. In the limit of weak absorption, light does not affect atoms in the ground state. All the ground state magnetic sublevels remain equally populated, and no coherences between magnetic sublevels in the ground state are created. In this situation, the density matrix of the excited state can be calculated as [14]

$$f_{mm'} = \frac{\Gamma_p}{\Gamma}\sum_{\mu}\langle F_e m|\hat{\mathbf{E}}^*_{exc}\cdot\hat{\mathbf{d}}|F_g\mu\rangle\langle F_e m'|\hat{\mathbf{E}}^*_{exc}\cdot\hat{\mathbf{d}}|F_g\mu\rangle^*. \quad (1)$$

A transition takes place from the ground-state hyperfine level $F_g$ to the excited-state hyperfine level $F_e$. Magnetic quantum numbers of the ground-state hyperfine level $F_g$ are denoted by $\mu$, and magnetic quantum numbers of the excited-state hyperfine level $F_e$ are denoted by $m$ and $m'$. Matrix elements of the dot product can be written as [15]

$$\langle F_e m|\hat{\mathbf{E}}^*\cdot\hat{\mathbf{d}}|F_g\mu\rangle = \sum_q (E^q)^*\langle F_e m|d^q|F_g\mu\rangle, \quad (2)$$

where $E^q$ are cyclic components of the polarization vector of light. These components, which in the general

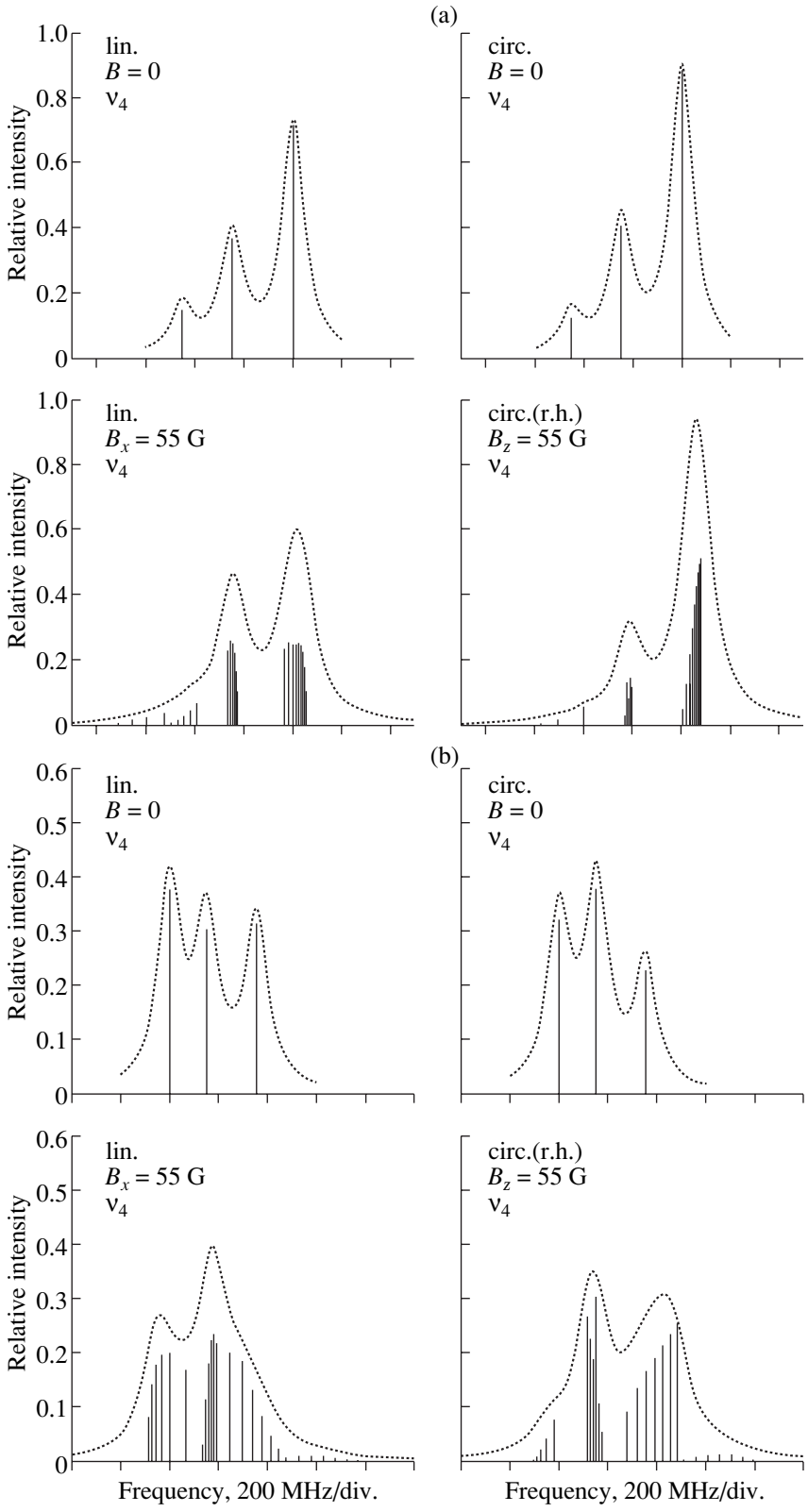


**Fig. 6.** Illustration of the simulation of the fluorescence spectrum for (a) $\nu_4$ and (b) $\nu_3$ transitions. Vertical bars show the relative strength of the individual fluorescence components $|F_e m\rangle \longrightarrow |F_g \mu\rangle$ for $B = 0$ (upper row) and $|\gamma_k m\rangle \longrightarrow |\eta_j \mu\rangle$ for $B = 55$ Gauss, (lower row). Dashed lines represent the sum of these (broadened) components.

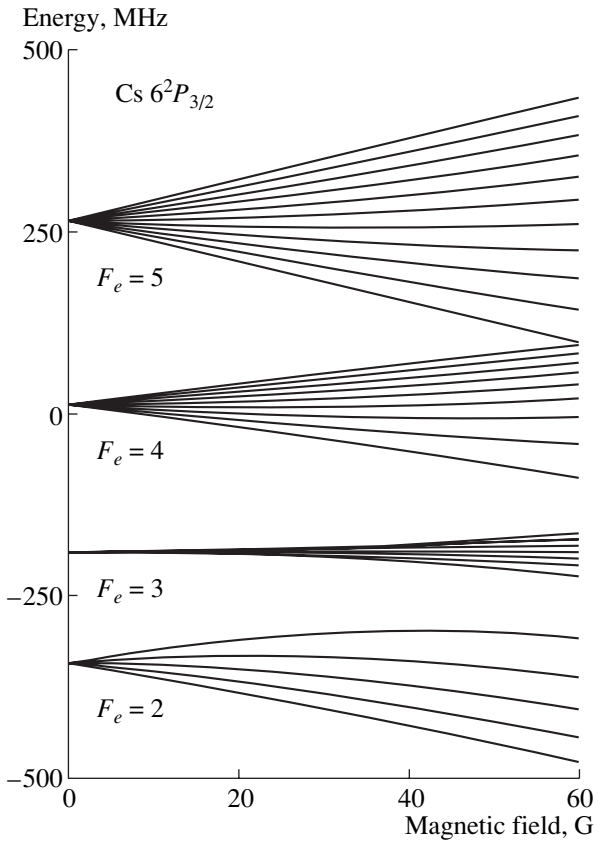


**Fig. 7.** Splitting and shift of the hyperfine states of the $6^2P_{3/2}$ level in a magnetic field.

case are complex numbers, are connected with more familiar Cartesian components as follows [13, 15]:

$$E^{+1} = -\frac{1}{\sqrt{2}}(E_x - iE_y),$$
$$E^0 = E_z, \qquad (3)$$
$$E^{-1} = \frac{1}{\sqrt{2}}(E_x + iE_y).$$

The remaining matrix element $\langle F_e m|d^q|F_g\mu\rangle$ can be written in an explicit form by means of the Wigner–Eckart theorem [15–17]:

$$\langle F_e m|d^q|F_g\mu\rangle = (-1)^{F_e - m}\begin{pmatrix} F_e & 1 & F_g \\ -m & q & \mu \end{pmatrix}\langle F_e\|d\|F_g\rangle, \quad (4)$$

where $\begin{pmatrix} \circ & \circ & \circ \\ \circ & \circ & \circ \end{pmatrix}$ is a 3-*jm* symbol. To calculate the reduced matrix element $\langle F_e\|d\|F_g\rangle$, we will assume the following scheme of formation of hyperfine-level angular momentum in ground and excited states:

$$\mathbf{J}_g + \mathbf{I} = \mathbf{F}_g; \quad \mathbf{J}_e + \mathbf{I} = \mathbf{F}_e, \qquad (5)$$

where $\mathbf{J}_g$ and $\mathbf{J}_e$ denote the total electronic angular momentum of an atom in the ground and excited states (including electron spin **S**) and **I** is the nuclear-spin angular momentum. This scheme allows one to write the angular part of the wavefunctions of an atom in the following form:

$$|F_g\rangle = |(J_g I)F_g\rangle, \quad |F_e\rangle = |(J_e I)F_e\rangle.$$

Therefore, taking into account that the transition dipole moment operator acts only on the electronic angular momentum and does not act on the nuclear-spin angular momentum, we obtain the following expression for the remaining reduced matrix element [16, 17]:

$$\langle F_e\|d\|F_g\rangle = (-1)^{J_g + I + F_e + 1}$$
$$\times\sqrt{(2F_e+1)(2F_g+1)}\begin{Bmatrix} J_g & F_g & I \\ F_e & J_e & 1 \end{Bmatrix}\langle J_e\|d\|J_g\rangle, \qquad (6)$$

where $\begin{Bmatrix} \circ & \circ & \circ \\ \circ & \circ & \circ \end{Bmatrix}$ is a 6*j* symbol. These last formulas make it possible to calculate the excited-state density matrix for different ground- and excited-state hyperfine levels.

Finally, the fluorescence signal for each allowed hyperfine transition from the excited-state hyperfine level $F_e$ to the final hyperfine level $F_g$ (which may or may not coincide with the level from which absorption took place) can be calculated according to [13] as

$$I = \tilde{I}_0 \sum_{mm'\mu}\langle F_e m|\hat{\mathbf{E}}^*_{\text{obs}}\hat{\mathbf{d}}|F_g\mu\rangle$$
$$\times\langle F_e m'|\hat{\mathbf{E}}^*_{\text{obs}}\hat{\mathbf{d}}|F_g\mu\rangle^* f_{m'm}, \qquad (7)$$

where $\mathbf{E}_{\text{obs}}$ denotes the polarization of light to which the detector is sensitive. In the case of fluorescence, the general approach to calculating the dipole transition matrix elements entering into Eq. (7) is the same as the above method for calculating matrix elements entering into Eq. (1) for the excited-state density matrix calculation. If we measure the total intensity of fluorescence on transitions to all ground-state hyperfine levels without discrimination for a specific light polarization, then we must simply take the sum of two fluorescence components with orthogonal polarizations observed in a definite direction and the sum of two spectral transitions to both the ground-state hyperfine levels with $F_g = 3$ and $F_g = 4$. Such a simulated spectrum for linearly and circularly polarized excitation is given in Fig. 6. The left and right graphs of the upper rows refer to the absorption of linearly and circularly polarized

light, respectively, from the ground-state hyperfine levels $F_g = 4$ (case a) and $F_g = 3$ (case b). The dashed line represents the sum of three Lorentz-type curves centered around the respected hyperfine component frequency. The width of this Lorentz-type spectral line is chosen equal to 55 MHz. This width gives signals that fit well to those observed experimentally. For the experimental signal observed in this work, this width includes the laser linewidth, the absorption linewidth formed by the homogeneous linewidth (natural and collisional), and residual Doppler broadening. Of course, when we have a homogeneous linewidth combined with inhomogeneous broadening, the resulting line shape should be a Voigt contour, but, in order to make the model as simple as possible, the Lorentz-type line shape for each individual peak was chosen for producing Fig. 6. This assumes that the remaining Doppler broadening is smaller than the homogeneous linewidth. One can see that the relative intensities of spectral components in this simulation differ from the relative line strength, which can be calculated as [18]

$$W_{F_g \leftrightarrow F_e} = (2F_e + 1)(2F_g + 1)(2J_e + 1)(2J_g + 1) \times \begin{Bmatrix} J_g & F_g & I \\ F_e & J_e & 1 \end{Bmatrix}^2 \begin{Bmatrix} L_g & J_g & S \\ J_e & L_e & 1 \end{Bmatrix}^2, \quad (8)$$

where $L_g$ and $L_e$ are electron orbital momenta for the ground and excited states.

This difference has an obvious explanation. Since we are using polarized light to excite atoms, the excited-state spatial angular momenta distribution of atoms is anisotropic. This anisotropy is different for different types of transitions and depends on quantum numbers $F_g$ and $F_e$. It is especially sensitive to the quantity $\Delta F = F_g - F_e$. Radiation emission from excited-state hyperfine levels in a specific spatial direction differ because of this anisotropy, as do other factors, such as the transition strength. For a more detailed explanation of this effect, see, for example, [19, 20].

### *3.2. Signal with a Magnetic Field*

When an external magnetic field is applied, the Hamilton operator for the atom in a magnetic field can be written as

$$\hat{H} = \hat{H}_0 + \hat{H}_{HFS} - \boldsymbol{\mu}_\mathbf{J} \cdot \mathbf{B} - \boldsymbol{\mu}_\mathrm{I} \cdot \mathbf{B}, \quad (9)$$

where $\hat{H}_0$ is the Hamiltonian operator of an unperturbed atom, and $\hat{H}_{HFS}$ represents hyperfine interaction. The remaining two terms represent interaction of the electronic magnetic moment $\boldsymbol{\mu}_\mathbf{J}$ of an atom and the nucleus magnetic moment $\boldsymbol{\mu}_\mathbf{I}$ with the external magnetic field **B**. These magnetic moments are connected with the respective electronic and nuclear-spin angular moments **J** and **I** of the atom:

$$\boldsymbol{\mu}_\mathbf{J} = \frac{g_J \mu_B}{\hbar}\mathbf{J}, \quad \boldsymbol{\mu}_\mathbf{I} = \frac{g_I \mu_0}{\hbar}\mathbf{I}, \quad (10)$$

where $\mu_B$ and $\mu_0$ are the Bohr and nuclear magnetons respectively and $g_J$, $g_I$ are electrotonic and nuclear Landé factors. The action of a magnetic field on the atom has two closely related effects. First, magnetic sublevels of the hyperfine levels are mixed in the magnetic field:

$$|\gamma_k m\rangle = \sum_{F_e = J_e - I}^{F_e = J_e + I} C^{(e)}_{kF_e}(B, m)|F_e, m\rangle,$$
$$|\eta_j \mu\rangle = \sum_{F_i = J_i - I}^{F_i = J_i + I} C^{(i)}_{jF_i}(B, \mu)|F_i, \mu\rangle, \quad (11)$$

where $C^{(e)}_{kF_e}(B, m)$ and $C^{(i)}_{jF_i}(B, \mu)$ are mixing coefficients depending on the field strength and magnetic quantum number ($m$ or $\mu$). The second effect is the deviation of the Zeeman magnetic sublevel splitting in the magnetic field from linear behavior. This means that the additional energy of the magnetic sublevel obtained in the magnetic field is no longer linearly proportional to the field strength. In the general case, new atomic states $|\gamma_k m\rangle$ and $|\eta_j \mu\rangle$ in the magnetic field are linear combinations of all initial hyperfine levels (four in the case of Cs atoms in the $6^2P_{3/2}$ state, and two in the case of Cs atoms in the $6^2S_{1/2}$ state). As can be seen from Eq. (11), the hyperfine angular-momentum quantum number $F$ ceases to be a good quantum number in the magnetic field but magnetic quantum numbers $m$ and $\mu$ are still good quantum numbers. This reflects the symmetry of the perturbation imposed by the magnetic field and means that only hyperfine sublevels with the same magnetic quantum numbers are mixed by the magnetic field.

The mixing coefficients $C^{(e)}_{kF_e}(B, m)$ and $C^{(i)}_{jF_i}(B, \mu)$ of the hyperfine states in the magnetic field and the energies of these levels ${}^{\gamma_k}E_m$, ${}^{\eta_j}E_\mu$ can be found as eigenvectors and eigenvalues of the Hamilton matrix (9). In Fig. 7, the energy levels obtained by Hamilton matrix diagonalization for Cs atoms in the excited $6^2P_{3/2}$ state in a magnetic field are presented.

For Cs atoms in the ground state, hyperfine level splitting exceeds 9 GHz, which is large in comparison to the magnetic sublevel energies obtained in the magnetic field. As a result, ground-state energy levels in the magnetic field can be very well approximated by the linear Zeeman effect. Namely, ${}^{\eta_j}E_\mu = g_{\eta_j}\mu_B B\mu/\hbar$, where $g_{\eta_j}$ is the Landé factor of the respective hyperfine level. For very weakly mixed levels, they can still

be represented with the hyperfine quantum number $F_g$. For Cs atoms in the $6^2S_{1/2}$ state, we have $g_{\eta_j} = -1/4$ for $F_g = 3$ and $g_{\eta_j} = 1/4$ for $F_g = 4$. In the case of mixing of only two hyperfine levels, an analytical formula can be derived for mixing coefficients and for level energies in the magnetic field that is similar to the Breit Rabi formula (see, for example, [21]).

The excited-state density matrix created by the laser light in the magnetic field can be written as (see for example [2])

$$
{}^{kl}f_{mm'} = \frac{\tilde{\Gamma}_p}{\Gamma + i^{kl}\Delta\omega_{mm'}} \times \sum_{j\mu} \langle \gamma_k m|\hat{\mathbf{E}}^*_{\text{exc}} \cdot \hat{\mathbf{D}}|\eta_j\mu\rangle\langle\gamma_l m'|\hat{\mathbf{E}}^*_{\text{exc}} \cdot \hat{\mathbf{D}}|\eta_j\mu\rangle^*, \tag{12}
$$

where ${}^{kl}\Delta\omega_{mm'} = ({}^{\gamma_k}E_m - {}^{\gamma_l}E_{m'})/\hbar$ is the energy splitting of the magnetic sublevels $m$ and $m'$ belonging to the excited-state levels $k$ and $l$. Magnetic quantum numbers of the ground-state level $\eta_j$ are denoted by $\mu$, and magnetic quantum numbers of the excited-state level $\gamma_{k,l}$ are denoted by $m$ and $m'$. In this last expression, it is assumed that two magnetic sublevels of the excited state that initially belong to two different hyperfine levels can have the same energy and can be excited simultaneously and coherently at some specific magnetic field strength. This means that nonzero field level crossing signals [2] are included in this model. However, for the practical calculations performed in this work, this is of no relevance, since no nonzero magnetic field level crossings of the magnetic sublevels initially belonging to different $F_e$ levels take place at the values $B \leq 55$ Gauss used in the experiment.

In our particular simulation, we assume that, when we scan the laser frequency in the manifold of splitted magnetic sublevels, only those transitions that are in exact resonance with the laser field are excited. So, at each radiation frequency, a specific density matrix is calculated. Of course, the density matrix is dependent on the magnetic field strength, which determines the magnetic sublevel splitting and wavefunction mixing and, as a result, transition probabilities between magnetic sublevels.

In the general case, the intensity of the fluorescence with a specific polarization $\mathbf{E}_{\text{obs}}$ in a transition between the excited $\gamma_k$ and final $\eta_j$ state in the magnetic field can be calculated according to [2] as

$$
I(\mathbf{E}_f) = I_0 \sum_{mm'\mu} \sum_{klj} \langle \gamma_k m|\hat{\mathbf{E}}^*_{\text{obs}} \cdot \hat{\mathbf{D}}|\eta_j\mu\rangle \times \langle\gamma_l m'|\hat{\mathbf{E}}^*_{\text{obs}} \cdot \hat{\mathbf{D}}|\eta_j\mu\rangle^{*kl} f_{mm'}. \tag{13}
$$

The final state of the fluorescence transition may or may not coincide with the atomic ground state from which the absorption started. In the lower row graphs in Fig. 6, the fluorescence spectra (line positions and relative intensities) are shown as vertical bars for the case of excitation from $F_g = 4$ (a) and $F_g = 3$ (b) with linear and circular light polarization. The dashed lines again show the resulting spectra, supposing that each component has a Lorentz line shape with 55 MHz in width. The results for $B = 55$ Gauss in Figs. 6 represent a graphical illustration of the calculation approach for the case of elementary polarizations ($\pi$, $B = B_x$, and $\sigma^+$, $B = B_z$). For other geometrical configurations, the situation is too complex to be presented by vertical bars, since two or even three elementary polarization components may be involved.

This approach to calculating spectra in a magnetic field and in the absence of a field was used in the simulation of experimentally observed signals. Simulation was performed for all the experimentally recorded spectra shown in Figs. 3–5; the results are presented as solid lines. One observes rather good agreement between the theoretical and experimental results. Some discrepancy observable in the graphs may be attributed to the following factors. First, the simulation model implies a Lorentz profile, rather than a Voigt one, for individual transitions, and this simplification may introduce some spectral distortions. Second, the cell geometry (narrow gap between thick windows) imposes additional (polarization-sensitive) asymmetry on the spatial distribution of the emission. The fluorescence emitted under the noticeable range of angles around 90° may be guided towards the photodiode by [multiple] grazing reflections from the external/internal faces of the window. Third, the recorded spectra may be affected by anisotropic elastic collisions of polarized atoms with the cell walls.

## 4. CONCLUSIONS

The resonance fluorescence of a Cs vapor layer of submicron thickness has been studied in the presence of a moderate (~50 Gauss) external magnetic field under excitation of atoms by laser radiation tuned to the frequency region of the D2 line. The spectra recorded for various reciprocal orientations of the magnetic field and laser polarization (linear, circular) exhibit a substantial frequency shift and modification of the peak amplitude and line shape for individual hyperfine transitions. These changes originate from mixing of the hyperfine levels of the upper state $6^2P_{3/2}$ and become observable because of the intrinsic sub-Doppler nature of an atomic signal in an extremely thin cell. Simulation has been performed by means of a quantum density matrix in the broad line approximation for a weak absorption regime, taking into account the mixing of magnetic sublevels of the hyperfine levels and their nonlinear shift in a magnetic field. The results of simulation show good agreement with the experimental results, which indicates that other possible effects

(anisotropy in long-range atom-surface interaction, coherent and propagation effects, etc.) do not contribute significantly in the conditions of our study.

Zeeman splitting of hyperfine sublevels in vapor media for moderate magnetic field strengths has been observed in selective reflection [4] and saturated absorption [22] spectroscopy. Nevertheless, direct recording of fluorescence (and possibly absorption) spectra using extremely thin cells is a more straightforward method, since the signal in this case is not influenced by contributions from other unavoidable processes (dispersion and nonlinear effects, crossover resonances, etc.). Sub-Doppler resolution, which is a necessary condition for the observation of Zeeman splitting, is satisfied also for atomic beams and for cold atoms. In these cases, however, cumbersome optical setups are required. Moreover, the application of a magnetic field may perturb the initial properties of the atomic system (the case of cold atoms in magnetooptical traps).

The results of the present work can be used for high spatial resolution magnetometry. Indeed, the interaction of laser radiation with an atomic system responsible for magnetic sensitivity takes place in the submicron gap between the cell windows. Note also that the transverse dimensions of the interaction region can be essentially reduced (to the micrometer range) by focusing the laser beam. The extremely small sensor size of the corresponding magnetometer device may allow fine mapping of the magnetic field spatial distribution, which could be important for many applications, in particular, for testing high-gradient magnetic fields. The magnetic field sensitivity can be noticeably enhanced by using the Rb D2 line, where a smaller splitting of the upper state ($5^2P_{3/2}$) will cause recordable level mixing effects at much lower $B$ fields (~1 Gauss). It should be noted that, although the suggested device will have much lower sensitivity than other optical magnetometer schemes (in particular, ones based on nonlinear Faraday and Hanle effects), there are several advantages that justify its possible application: (i) a unique spatial resolution, (ii) simplicity of the optical setup, and (iii) an extended upper limit of measured $B$ fields.

## ACKNOWLEDGMENTS

This work was supported, in part, by grants nos. 00-378 and 00-381 of the Ministry of Economics of Armenia, as well as by ANSEF grant no. PS 18-01. The authors are grateful to A. Sarkisyan for his valuable contribution to the fabrication of the ETCs and to Yu. Malakyan for stimulating discussions. The French-Armenian cooperation receives a specific support from CNRS (project no. 12856).

## REFERENCES

1. Tremblay, P., Michaud, A., Levesque, M., *et al.*, 1990, *Phys. Rev. A*, **42**, 2766.
2. Alnis, J. and Auzinsh, M., 2001, *Phys. Rev. A*, **63**, 023407.
3. Weis, A., Sautenkov, V.A., and Hänsch, T.W., 1993, *J. Phys. II*, **3**, 263.
4. Papageorgiou, N., Weis, A., Sautenkov, V.A., *et al.*, 1994, *Appl. Phys. B*, **59**, 123.
5. Chen, X., Telegdi, V.L., and Weis, A., 1987, *J. Phys. B: At. Mol. Phys.*, **20**, 5653.
6. Auzinsh, M., Stolyarov, A.V., Tamanis, M., and Ferber, R., 1996, *J. Chem. Phys.*, **105**, 37.
7. Auzinsh, M., 2001, *Phys. Scr.*, **95**, 12.
8. Sarkisyan, D., Bloch, D., Papoyan, A., and Ducloy, M., 2001, *Opt. Commun.*, **200**, 201.
9. Briaudeau, S., Saltiel, S., Nienhuis, G., *et al.*, 1998, *Phys. Rev. A*, **57**, R3169.
10. Zambon, B. and Nienhuis, G., 1997, *Opt. Commun.*, **143**, 308.
11. Theodosiou, C.E., 1984, *Phys. Rev. A*, **30**, 2881.
12. Ducloy, M., 1973, *Phys. Rev. A*, **8**, 1844.
13. Auzinsh, M. and Ferber, R., 1995, *Optical Polarization of Molecules* (Cambridge: Cambridge Univ. Press).
14. Tamanis, M., Auzinsh, M., Klincare, I., *et al.*, 1997, *J. Chem. Phys.*, **106**, 2195.
15. Varshalovich, D.A., Moskalev, A.N., and Khersonskii, V.K., 1988, *Quantum Theory of Angular Momentum* (Singapore: World Sci.).
16. Sobelman, I.I., 1979, *Atomic Spectra and Radiative Transitions* (Berlin: Springer).
17. Zare, R.N., 1988, *Angular Momentum* (New York: Wiley).
18. Alnis, J. and Auzinsh, M., 2001, *J. Phys. B: At. Mol. Opt. Phys.*, **34**, 3889.
19. Theobald, G., Dimarcq, N., Giordano, V., *et al.*, 1989, *J. Appl. Phys.*, **66**, 4581.
20. Auzinsh, M., 1997, *Can. J. Phys.*, **75**, 853.
21. Aleksandrov, E.B., Chaika, M.P., and Khvostenko, G.I., 1993, *Interference of Atomic States* (New York: Springer).
22. Schmidt, O., Knaak, K.-M., Wynands, R., and Meschede, D., 1994, *Appl. Phys. B*, **59**, 167.